SCIENCE CHINA
Information Sciences

• RESEARCH PAPER •

April 2016, Vol. 59 042410:1–042410:10
doi: 10.1007/s11432-015-5454-z

Novel high voltage RESURF AlGaN/GaN HEMT with charged buffer layer

Jiayun XIONG, Chao YANG, Jie WEI, Junfeng WU, Bo ZHANG & Xiaorong LUO*

State Key Laboratory of Electronic Thin Films and Integrated Devices, University of Electronic Science and Technology of China, Chengdu 610054*, China*

Received August 6, 2015; accepted September 15, 2015; published online February 17, 2016

Abstract A novel reduced surface field (RESURF) AlGaN/GaN high electron mobility transistor (HEMT) with charged buffer layer is proposed. Its breakdown mechanism and on-state characteristics are investigated. The HEMT features buried Fluorine ions in the GaN buffer layer both under the Drift and the Gate region (FDG). The section of FDG under the drift region (FD) not only reduces the electric field (E-field) peak at the gate edge but also enhances the E-field in the drift region by the assisted depletion, leading to a significant improvement in breakdown voltage (BV). Moreover, the section of FDG under the gate (FG) enhances the back barrier and effectively prevents electron injecting from the source to form leakage current, thus a higher BV is achieved. The BV of the proposed HEMT sharply increases to 750 V from 230 V of conventional AlGaN/GaN HEMT with the same dimensional parameters, and the specific on-resistance ($R_{\mathrm{on,sp}}$) just increases to 1.21 mΩ·cm^2 from 1.01 mΩ·cm^2.

Keywords high voltage, power device, AlGaN/GaN HEMT, charged buffer, RESURF

Citation Xiong J Y, Yang C, Wei J, et al. Novel high voltage RESURF AlGaN/GaN HEMT with charged buffer layer. Sci China Inf Sci, 2016, 59(4): 042410, doi: 10.1007/s11432-015-5454-z

1 Introduction

AlGaN/GaN high-electron-mobility transistors (HEMTs) are emerging as promising candidates for next generation microwave power amplifiers and high-voltage switches owing to their superior properties such as high two-dimensional electron gas (2DEG) density, high electron saturation velocity, and high critical breakdown electric field (E-field) [1,2]. Thus, high breakdown voltage (BV) can be realized in AlGaN/GaN HEMTs with ultralow on-resistance, breaking through the Si-limit [3]. However, the reported BV and output power of the devices are still far lower than the theoretical limit of GaN.

In the off-state, electrons could be injected from the source to the high E-field region through the buffer and initiate the impact ionization, leading to breakdown [4]. To modulate the E-field distribution and suppress the buffer leakage, several technologies have been employed, including the field plate (FP) [5], carbon-doped buffer [6], AlGaN back barrier [7], p-type doped buffer [8] and Schottky contacts in the source [9]. However, the FP will induce an additional parasitic capacitance. Carbon doping in the

* Corresponding author (email: xrluo@uestc.edu.cn)

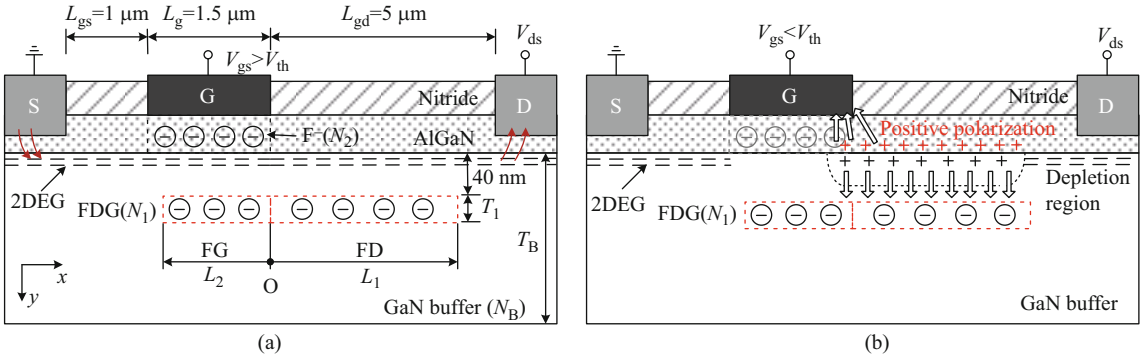

Figure 1 (Color online) Schematic cross section of the proposed FDG-HEMT in (a) ON-state, and (b) OFF-state.

buffer may cause the current collapse [10]. The other ways used to restrict the premature breakdown may induce significant negative impact on the on-state performance.

The fluorine ions (F^-) treatment in AlGaN/GaN HEMTs and its stability were theoretically and experimentally investigated [11–15]. Most of them are used to realize the normally-off mode [11–12]. The F^- implanted in the AlGaN barrier layer is also used to improve the BV [13–14]. However, the F^- was implanted in the thin AlGaN barrier layer (∼20 nm) between the gate and drain. Thus the F^- easily induces damage to the 2DEG channel. The on-state performance and reliability will be degraded and the BV cannot be optimized to the best level. The F^- implantation in the buffer layer just under the gate was also experimentally carried out to alleviate the drain induced barrier lowering (DIBL) effect [15].

In this paper, a novel reduced surface field (RESURF) AlGaN/GaN HEMT with buried F^- in the buffer layer both under the Drift region and the Gate (FDG) is proposed and its off-state as well as on-state electrical performances are investigated. Simulation indicates that the FDG can significantly improve the BV with little impact on the maximum drain current ($I_{d,max}$) and specific on-resistance ($R_{on,sp}$).

2 Device structures and mechanism

Figure 1(a) is the schematic cross section of the proposed HEMT. The HEMT features a buried Fluorine ions layer in the GaN buffer under the Drift and the Gate region (FDG-HEMT). L_1 and L_2 are the length of the FDG under the drift region (FD) and under gate region (FG) respectively. The L_1 lengthens from point O to the drain, and the L_2 lengthens from O to the gate left edge. When L_2=0 and $L_1 \neq 0$, the device structure is just with FD and called as FD-HEMT, which is also first proposed in this paper. When L_2=0 and L_1=0, the structure is the conventional HEMT (C-HEMT). The distance from the FDG to the AlGaN/GaN interface is 40 nm which is referred on experiment [15]. The uniform doped FDG is used to modulate the physical mechanism of the F^- implantation in the buffer layer. The N_1 and T_1 are the concentration and thickness of the FDG. The F^- in the AlGaN barrier layer under the gate is used in the three types of HEMTs to realize the enhancement-mode (E-mode), with the concentration of N_2. All the three HEMTs have 1 μm gate-source distance (L_{gs}), 1.5μm gate length (L_g), 5 μm gate-drain distance (L_{gd}), 200-nm-thick Si_3N_4 passivation on the AlGaN, 25-nm-thick $Al_{0.26}Ga_{0.74}N$ barrier, 1.5-μm-thick (T_B) GaN slightly n-type doped (N_B=1×10^{15} cm^{-3}) buffer layer on sapphire substrate. The net acceptor (deep level) density in the buffer layer is set to be 1.5×10^{16} cm^{-3} and the energy level is 0.45 eV below the conduction band minimum [16]. The x and y direction are given.

Figure 1(b) indicates the buried F^- depletes the 2DEG in the drift region at off-state, the FD extends the depletion region and the FG prevents electron injecting from the source, which optimizes the E-Field distribution and enhances the BV. The E-field lines not only terminate in the gate electrode but also terminate in the FDG. As a result, the peak E-field around the gate edge is decreased and the E-field in the drift region is enhanced, yielding the RESURF effect.

The physical mechanism is analyzed based on 2D Sentaurus TCAD from Synopsys. The simulations

Table 1 Some physical properties of GaN and AlN [18]

Material	GaN	AlN
E_g(eV)	3.4	6.03
ε_0	9.0	8.5
Lattice constant (A)	3.186	3.112
$\mu_{e,max}$(cm^2/Vs)	1460	300
μ_h(cm^2/Vs)	22	14
v_s(10^7 cm/s)	2.5	2.2

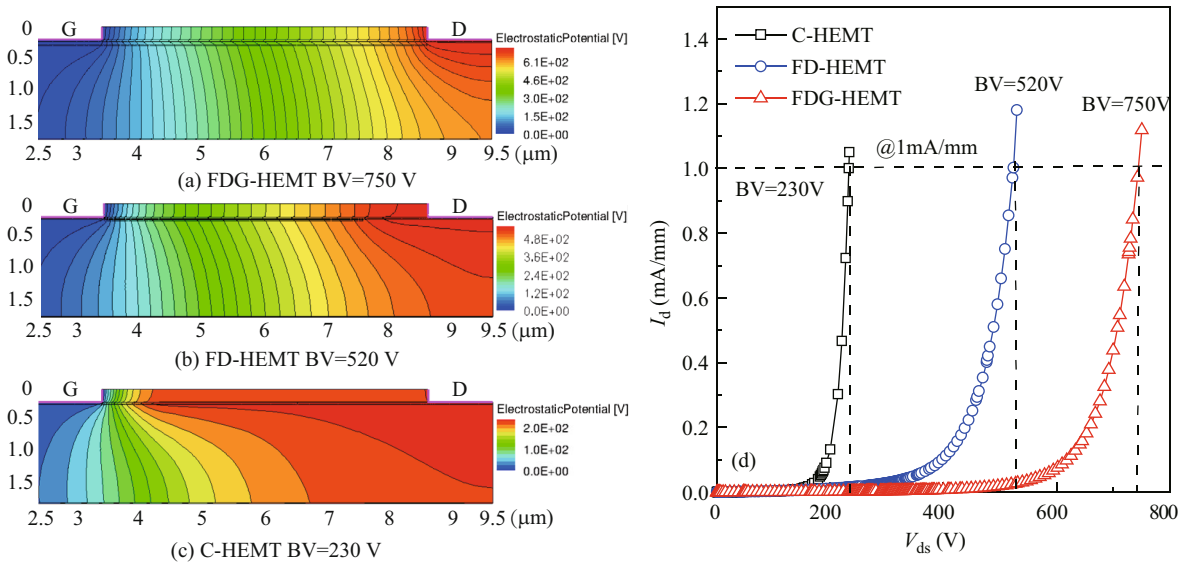

Figure 2 (Color online) (a)–(c) Equipotential contours at breakdown (20V/contour), (d) I-V curves, where the BV is defined as the source-drain voltage at I_d=1 mA/mm, V_{gs}=0 V.

use Drift–Diffusion (DD) model, Overstraeten–de Man and Canali model [17]. Several important physical effects such as bandgap narrowing, doping dependent mobility and spontaneous polarizations are also accounted in simulations. Table 1 shows some physical properties of GaN and AlN. The physical properties of the $Al_xGa_{1-x}N$ in simulation are calculated from GaN (x=0) and AlN (x=1) nonlinearly.

Figure 2 compares the potential lines distribution among the FDG-, FD- and C- HEMT at breakdown. In Figure 2(a) and 2(b), the FD extends the depletion region in the drift region and increases the average E-field strength, resulting in the uniform potential line distribution. Comparison of Figure 2(a) with Figure 2(b) shows that the FG restricts the electrons injection from the source to form leakage current. Therefore, the BV of the FDG-HEMT increases to 750 V from 520 V of FD-HEMT. However, without the FD and FG for the C-HEMT, the drift region cannot be fully depleted and all potential contours are collected at the gate edge, wherein E-field concentrates and the electrons inject to the high field region through the buffer easily. Thus the highest BV (230 V) of the C-HEMT is reached at L_{gd}=3 μm with the increase in the L_{gd}. The I-V curves at breakdown are compared in Figure 2(d).

Figure 3 shows the E-field distributions at breakdown. Owing to the E-field modulation and the charge sharing caused by the RESURF effect, the x-component of lateral E-field (E_x) distributions of the FDG-HEMT and FD-HEMT are more uniform and higher than that of the C-HEMT as shown by red and blue area in Figure 3(a). First, the depletion width and the E-field strength in the drift are enhanced due to the assisted-depletion caused by the FD. Second, the peak E-field around the gate edge is decreased by comparing the FD-HEMT with C-HEMT. Third, the FDG-HEMT allows a higher E-field strength near the gate at breakdown than FD-HEMT because the FG prevents the electrons from injecting to cause large leakage current. An approximately linear potential is shown in the inset of Figure 3(a) for the FDG-HEMT. In Figure 3(b), the charge sharing in the y direction is verified by the large E-field y-component (E_y). In the y-direction, both the depletion width and the E-field strength of the FDG-

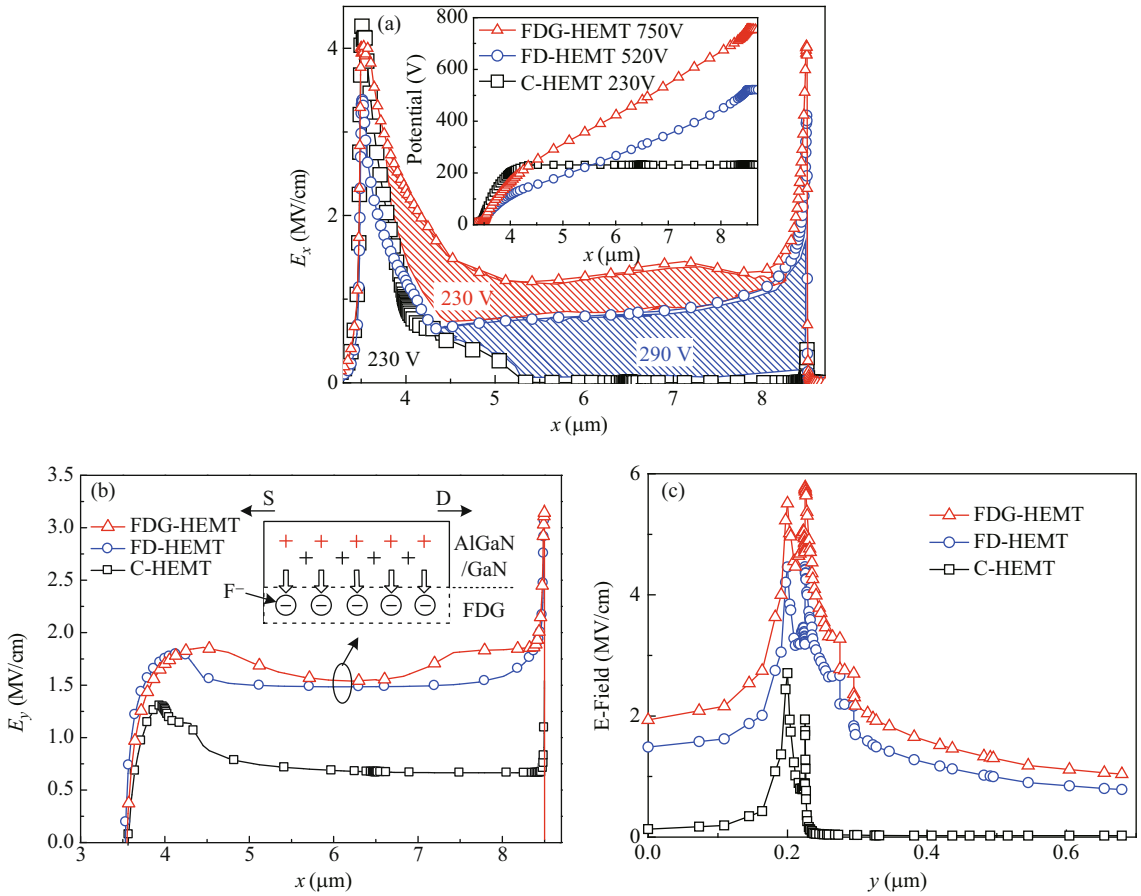

Figure 3 (Color online) E-field distribution of the three types HEMTs at breakdown. (a) x-component of the lateral E-field distribution at y=0.226 μm (in the 2DEG channel), and the inset depicts the potential distribution; (b) y-component of the lateral E-field distribution; (c) vertical E-field distribution at the drain side (x=8.49 μm).

HEMT are highest, as shown in Figure 3(c). Therefore, the FDG improves the lateral and vertical E-field distributions, resulting in an enhanced BV.

Figure 4(a) demonstrates the conduction band profile along the x-direction at different depth and different N_1. The built-in potential between the FG and n-type GaN buffer layer (at y=0.25 μm) is $\phi_{\rm b}$. $\phi_{\rm b}$ increases with the increasing N_1 as depicted in Figure 4(a) and Eq. (1). Due to the coupling effect of the FG, the barrier heights at the channel (y=0.226 μm) and deep-buffer (y=0.5 μm) are also elevated compared with those at N_1=0. Therefore, the origin of the leakage current and the leakage current path are restricted. According to the thermionic-diffusion (T-D) emission theory, the buffer leakage current density ($J_{\rm buffer}$) is mainly determined by the barrier height $q\phi_{\rm b}$ and $V_{\rm ds}$ in Eq. (2). Thus the FG effectively lowers the $J_{\rm buffer}$, leading to a higher BV.

$$\phi_{\rm b} = \frac{kT}{q} \ln \frac{N_1 N_B}{n_i^2}, \tag{1}$$

$$J_{\rm buffer} = A \exp\left(-\frac{q\phi_{\rm b}}{kT}\right)\left[\exp\left(\frac{q\lambda V_{\rm ds}}{kT}\right) - 1\right], \tag{2}$$

where A is the Richard constant, N_B and N_1 are the concentration of GaN buffer layer and FDG respectively, $\lambda < 1$ indicates that only a part of the $V_{\rm ds}$ potential drop affects the barrier height. Figure 4(b) demonstrates the conduction band profile along the x-direction at different $V_{\rm ds}$. For the FD-HEMT, there is a barrier $q\phi_{\rm b}'$ between the FD and n-type GaN buffer layer.

Figure 5 shows the leakage current distribution for the three HEMTs at $V_{\rm ds}$=230 V which is the BV of the C-HEMT. For the FDG-HEMT, the electron injection from the source is effectively restricted

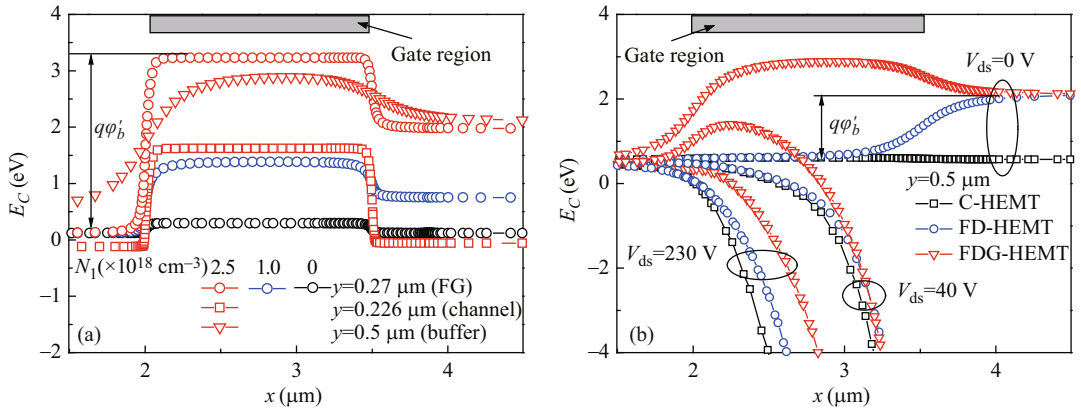

Figure 4 (Color online) (a) Lateral conduction band profile at y=0.226 μm, y=0.27 μm, y=0.5 μm with different N_1. (b) Lateral conduction band profile in the GaN buffer layer y=0.5 μm for the FDG-, FD- and C- HEMT.

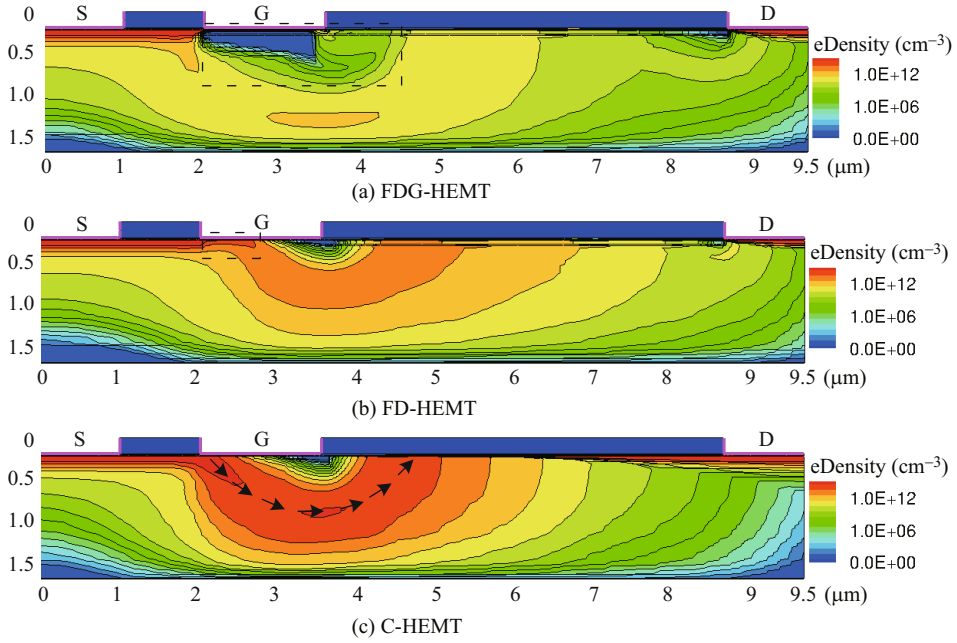

Figure 5 (Color online) Leakage current density contours at V_{ds}=230 V (1 order of magnitude/contour). (a) FDG-HEMT; (b) FD-HEMT; (c) C-HEMT.

as shown by the dashed rectangle in Figure 5(a). For the FD-HEMT, the absence of the FG provides a window for leakage current as shown in the dashed rectangle of Figure 5(b). Without the FD and FG for the C-HEMT, there is a continuous leakage current path of source-buffer-drift 2DEG channel as demonstrated by the arrow heads in Figure 5(c).

Figure 6 shows the conduction band profiles across the gate region (x=3 μm) and drift region (x= 4 μm) along the y-direction. The conduction band increment ΔE_1 as the enhanced back barrier not only restricts the source carrier injection, but also confines the 2DEG within the channel, reducing the leakage current. As for the gate region, the uplift of the conduction band in the AlGaN barrier layer will elevate the triangular well at the AlGaN/GaN interface [12]. Moreover, when the F^- in the AlGaN barrier layer is combined with the FG, the triangular well could be elevated by ΔE_2 further, causing a threshold voltage shift of +0.4 V. In the drift region, note that the FDG alone almost has no effect on the depth of the triangular well, as shown in Figure 6. Thus, the proposed FDG in the GaN buffer has insignificant impact on the $I_{d,max}$ and $R_{on,sp}$.

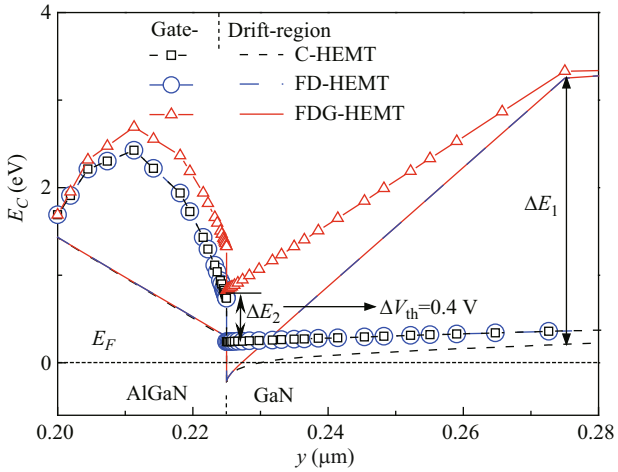

Figure 6 (Color online) Conduction band profile at gate region and drift region in the y-direction at V_{gs}=0 V. The effective n-type background doping in the buffer is 1×10^{15} cm^{-3}.

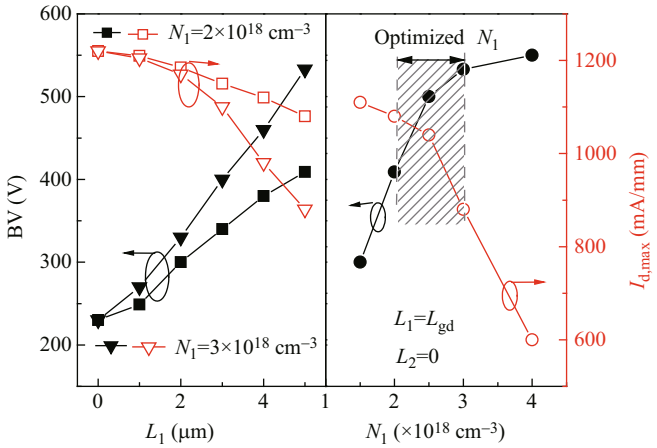

Figure 7 (Color online) Influence of N_1, L_1 on the BV and $I_{d,max}$.

3 Simulation results and discussion

Figure 7 shows the influences of the N_1, L_1 on the BV and $I_{d,max}$ at L_2=0. With the increases in the L_1, the BV increases owing to the expanded depletion region between the gate and drain. The $I_{d,max}$ decreases with the increasing L_1 and N_1 due to the increasing assisted depletion effect on the 2DEG.

For Silicon RESURF devices, the optimum dose is (1∼2)×10^{12} cm^{-2}. The optimum RESURF dose for GaN is expected to be 1×10^{13} cm^{-2} due to 10 times higher critical electric field [19]. The negatively charged F^- is used to realize the function of P-doped region. The F^- is implanted as effective fixed negative charges. However, the activity ratio of P type impurity in GaN is very low and the P-doped semiconductor needs to be depleted to form the effective negative space charges. When $L_1 = L_{gd}$, according to charge balance among the polarization charge, N-drift buffer region, and the FDG, we get the approximate RESURF criterion

$$N_B \times T_B + Q_{\text{polarization}} = N_1 \times T_1 \approx 1 \times 10^{13}\text{cm}^{-2}, \tag{3}$$

where T_1=40 nm, T_B=1.5 μm, N_B =2×10^{15} cm^{-3}. The polarization charge density $Q_{\text{polarization}}$ is equal to the dose of the 2DEG (Q_{2DEG}). For given T_1=40 nm, the optimized N_1=2.57×10^{18} cm^{-3} is calculated from Eq. (3), almost consistent with the result in Figure 7.

Figure 8 shows the influence of the L_2 on the BV and conduction band profile at $L_1 = L_{gd}$. With the increases in the L_2, the BV increases with the energy barrier expanding as indicated in Figure 8(b). The

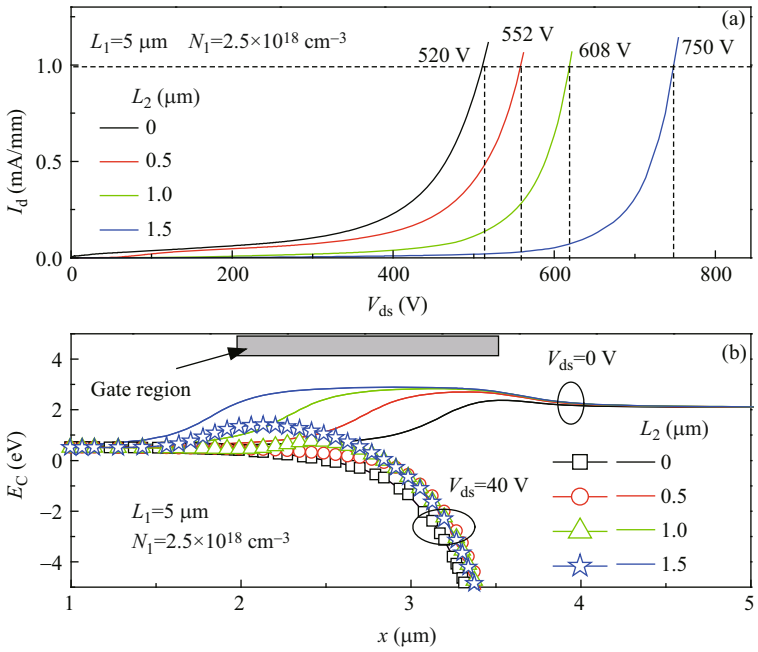

Figure 8 (Color online) (a) Influence of L_2 on BV; (b) conduction band profile at y=0.5 μm.

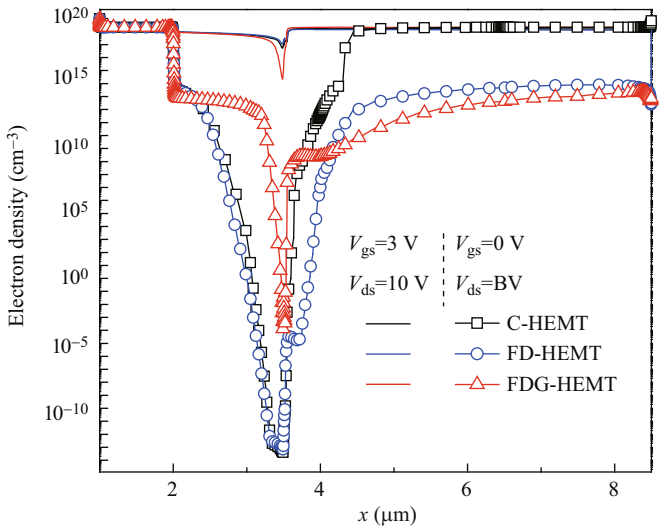

Figure 9 (Color online) Electron density in the 2DEG channel at on-state and at breakdown.

maximum BV is obtained at $L_2 = L_g$=1.5 μm. The FG region restricts the injection of the carrier from the source.

Figure 9 shows the 2DEG density at the on-state and off-state. The FDG has little effect on the 2DEG density at on-state. At the off-state V_{ds}=BV, the 2DEG density in the drift region for the C-HEMT keeps a high value, providing a leakage path. With the assisted-depletion caused by the FDG, the 2DEG density of the FD-HEMT and FDG-HEMT is decreased by five orders of magnitude as shown by the symbols in Figure 9. Therefore, the buffer layer leakage current from the drain to the source is reduced and a higher BV is achieved.

The transfer characteristic and output characteristic are compared in Figure 10. The three HEMTs are normally-off on the condition of N_2=7.6×10^{18} cm^{-3} in the AlGaN barrier. The V_{th} of the FDG-, FD- and C- HEMT are 1.4 V, 1 V and 1 V, respectively. The inset in Figure 10(a) shows that the Schottky gate of the three HEMTs turns on (I_g=1 mA/mm) at about V_{gs}=5.3 V (at $V_d = V_s$=0 V). The F^- in the AlGaN under the gate induces an electron barrier, restricting the electrons from the channel to the

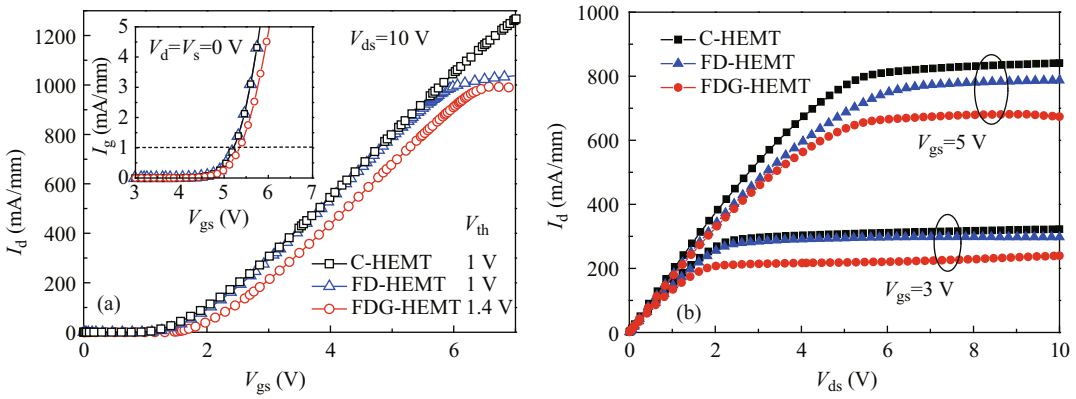

Figure 10 (Color online) (a) Transfer characteristics at V_{ds}=10 V, (b) I-V output characteristics (V_{gs}= 3 V, 5 V).

gate as shown in Figure 6. Thus the gate leakage current can be effectively reduced and the gate voltage swing can be expanded by the F implantation in the AlGaN. Moreover, the gate turn on voltage increases with the increase in the F dose [11]. The gate swing of the FDG-HEMT is slightly higher than that of the others due to the higher V_{th} caused by FG. Compared with those of the C-HEMT, the BV of the FDG-HEMT is increased by more than three times on the condition of decrease in $I_{d,max}$ only by 15% as shown in Figure 10(a). The On-Resistance (R_{on}) mainly consists of the channel resistance (R_{ch}) and the drift resistance (R_d). The R_{ch} depends on the V_{th} and V_{gs} while R_d relies on the 2DEG in the drift region. At the low V_{gs}, the R_{ch} plays an important role; on the contrary, R_d is the major part of the R_{on}. In Figure 10(b), the I_d of the FDG-HEMT is lowest and that of the other two HEMTs are almost the same at V_{gs}=3 V since the R_{ch} and V_{th} play a determined effect. As the V_{gs} increases, the I_d of the FDG-HEMT and FD-HEMT are increasingly closer because the R_d gets more important.

Figure 11 illustrates $R_{on,sp}$ and BV values of the three devices and recently reported AlGaN/GaN HEMTs, together with the theoretical Si- , SiC- and GaN- limit. The $R_{on,sp}$ of the FDG-, FD- and C-HEMT (at V_{gs}=5 V) are 1.21 mΩ·cm^2, 1.16 mΩ·cm^2 and 1.01 mΩ·cm^2 respectively. There is only slight degradation in the on-state characteristics because the concentration of the FDG is relatively low and the F^-implantation in the thick buffer layer induces little effect to the 2DEG. Moreover, according to the experiment in [11], the rapid thermal annealing (RTA) (400 °C for 10 min) can recover the 2DEG mobility and the lattice damages effectively. Note that the improvement of BV is more significant, compared with the increase of $R_{on,sp}$. As a result, an excellent trade-off between the off-state characteristics and the on-state characteristics is achieved.

Figure 12 shows the key fabrication steps of the FDG-HEMT. The process flow refers to the experiment [15]. After source/drain ohmic contact formation, the devices were treated by CF_4 plasma in an RIE system. In step (a) the FDG window of the FDG-HEMTs were implanted by F^- with energy of 50 keV at a dose of 1×10^{13} cm^{-2}, with a position of the peak concentration at about 40 nm. Although the F^- implantation in the GaN buffer passes through the AlGaN barrier and the 2GEG channel, the actual F^- profile as shown in the grey region induces acceptable negative effects to the forward performance, according to the experiment. Step (b) shows another higher dose F^- implantation in the AlGaN barrier. The implantation energy of F^- is 10 keV and the dose of F^- is 3×10^{13} cm^{-2} [12]. Then, the samples were annealed at 400°C for 15 min in N_2 ambient. Finally the Schottky gate is formed in step (c).

As we can see from Figure 12, the actual F^- concentration profile in experiment is approximate Gauss distribution. So the Gauss F^- profile is also simulated to compare with the uniform F^- profile discussed before. The peak concentration is 1.5×10^{18} cm^{-3} with a position at about 40 nm. Figure 13 shows the influence of F^- profile on the performance of the FDG-HEMT. With almost the same BV, the $I_{d,max}$ and $R_{on,sp}$ of the Gauss F^- profile are lower than those of the uniform F^- profile within an acceptable range.

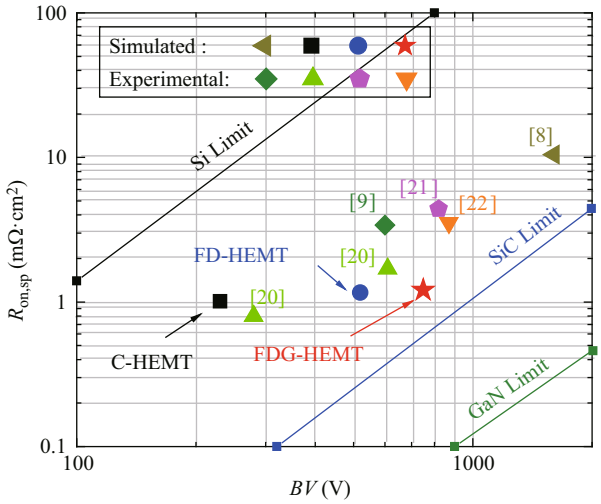

Figure 11 (Color online) $R_{on,sp}$ and off-state BV in the proposed devices and recently reported AlGaN/GaN HEMTs, together with the theoretical Si- , SiC- and GaN- limit.

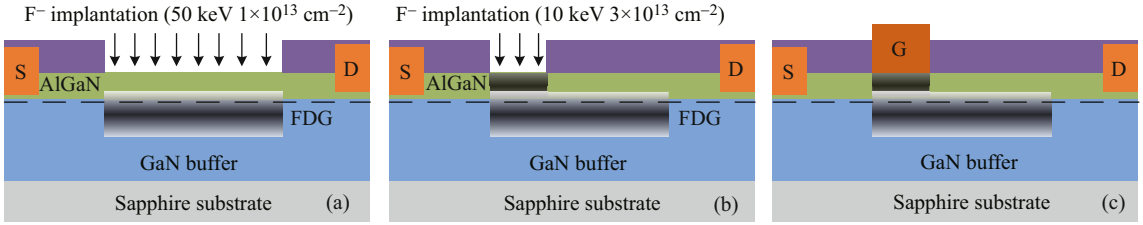

Figure 12 (Color online) Key process steps of the FDG-HEMT for forming (a) FDG; (b) F^- region in the barrier to realize the E-mode; (c) Schottky gate.

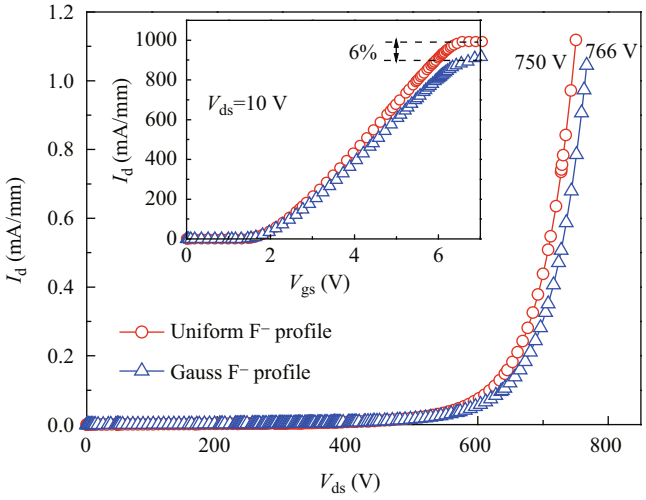

Figure 13 (Color online) Influence of F^- profile on the performance of the FDG-HEMT.

4 Conclusion

AlGaN/GaN HEMTs with the FDG in GaN buffer layer both under the drift and gate region are proposed and investigated by simulation. The FD yields a charge sharing effect in the y direction and modulates the E-field of the drift region, resulting in a uniform E-field distribution. Moreover, the FG effectively raises the back barrier and hence reduces leakage current. Thus the off-state BV is greatly improved by more than three times with insignificant degradation in on-state characteristics. The proposed devices

possess a better trade-off relationship between the BV and $R_{\mathrm{on,sp}}$. The FDG technique is available to achieve power devices with the capacity of high voltage, high output power and low power dissipation.

Conflict of interest The authors declare that they have no conflict of interest.

References

1 Paul C T, Ritu T. Wide bandgap compound semiconductors for superior high-voltage unipolar power devices. IEEE Trans Electron Dev, 1994, 41: 1481–1483
2 Ambacher O, Foutz B, Smart J, et al. Two dimensional electron gases induced by spontaneous and piezoelectric polarization in undoped and doped AlGaN/GaN heterostructures. J Appl Phys, 2000, 87: 334–343
3 Wataru S, Ichiro O, Tsuneo O, et al. Theoretical limit estimation of lateral wide band-gap semiconductor power-switching device. Solid-State Electron, 2004, 48: 1555–1562
4 Duan B X, Yang Y T. Breakdown voltage analysis for the new RESURF AlGaN/GaN HEMTs. Sci China Inf Sci, 2012, 55: 473–479
5 Wei K, Liu X Y, He Z J, et al. DC chacteristics of AlGaN/GaN HEMTs with a field plate gate. J Semiconduct, 2008, 57: 1492–1496
6 Eldad B T, Frank B, Oliver H, et al. AlGaN/GaN/GaN:C back-barrier HFETs with breakdown voltage of over 1 kV and low $R_{ON}\times A$. IEEE Trans Electron Dev, 2010, 57: 3050–3058
7 Eldad B T, Oliver H, Frank B, et al. Punchthrough-voltage enhancement of AlGaN/GaN HEMTs using AlGaN double-heterojunction confinement. IEEE Trans Electron Dev, 2008, 55: 3354–3359
8 Zhao Z Q, Zhao Z Y, Luo Q, et al. High-voltage RESURF AlGaN/GaN high electron mobility transistor with back electrode. Electron Lett, 2013, 49: 1638–1640
9 Zhou Q, Chen W J, Liu S H, et al. Schottky-contact technology in InAlN/GaN HEMTs for breakdown voltage improvement. IEEE Trans Electron Dev, 2013, 60: 1075–1081
10 Klein P B, Binari S C, Ikossi K, et al. Current collapse and the role of carbon in AlGaNÕGaN high electron mobility transistors grown by metalorganic vapor-phase epitaxy. Appl Phys Lett, 2001, 79: 3527–3529
11 Cai Y, Zhou Y G, Chen K J, et al. High-performance enhancement-mode AlGaN/GaN HEMTs using fluoride-based plasma treatment. IEEE Electron Dev Lett, 2005, 26: 435–437
12 Chen K J, Yuan L, Wang M J, et al. Physics of fluorine plasma ion implantation for GaN normally-off HEMT technology. In: Electron Devices Meeting (IEDM), San Francisco, 2010. 465–468
13 Song D, Liu J, Cheng Z, et al. Normally off AlGaN/GaN low-density drain HEMT (LDD-HEMT) with enhanced breakdown voltage and reduced current collapse. IEEE Electron Dev Lett, 2007, 28: 189–191
14 Young S K, Lim J Y, Seok O G, et al. High breakdown voltage AlGaN/GaN HEMT by employing selective fluoride plasma treatment. In: Proceedings of the 23rd International Symposium on Power Semiconductor Devices & IC's (ISPSD), San Diego, 2011. 251–255
15 Wang M J, Chen K J. Improvement of the off-state breakdown voltage with fluorine ion implantation in AlGaN/GaN HEMTs. IEEE Trans Electron Dev, 2011, 58: 460–465
16 Uren M J, Nash K J, Balmer R S, et al. Punch-through in short-channel AlGaN/GaN HFETs. IEEE Trans Electron Dev, 2006, 53: 395–398
17 Stephan S, Axel E, Tommaso C, et al. TCAD methodology for simulation of GaN-HEMT power devices. In: Proceedings of the 23rd International Symposium on Power Semiconductor Devices & IC's (ISPSD), Hawaii, 2014. 257–260
18 Bougrov V, Levinshtein M E, Rumyantsev S L, et al. Properties of Advanced Semiconductor Materials GaN, AlN, InN, BN, SiC, SiGe. New York: John Wiley & Sons, Inc. 2001. 1–30
19 Huang W, Chow T P, Niiyama Y, et al. Lateral implanted RESURF GaN MOSFETs with BV up to 2.5 kV. In: Proceedings of the 20rd International Symposium on Power Semiconductor Devices & IC's (ISPSD), Orlando, 2008. 291–294
20 Yuan L, Chen H W, Zhou Q, et al. A novel normally-off GaN power tunnel junction FET. In: Proceedings of the 23rd International Symposium on Power Semiconductor Devices & IC's (ISPSD), San Diego, 2011. 276–279
21 Park B R, Lee J G, Choi W, et al. High-quality ICPCVD SiO2for normally off AlGaN/GaN-on-Si recessed MOSHFETs. IEEE Electron Dev Lett, 2013, 34: 354–356
22 Hilt O, Knauer A, Brunner F, et al. Normally-off AlGaN/GaN HFET with p-type GaN Gate and AlGaN Buffer. In: Proceedings of the 22nd International Symposium on Power Semiconductor Devices & IC's (ISPSD), Hiroshima, 2011. 347–350